

## Fabricable dihedral Escher tessellations

Xiaokang Liu<sup>a</sup>, Lin Lu<sup>a,\*</sup>, Andrei Sharf<sup>b</sup>, Xin Yan<sup>a</sup>, Dani Lischinski<sup>c</sup>, Changhe Tu<sup>a</sup>

<sup>a</sup> School of Computer Science and Technology, Shandong University, Qingdao, China

<sup>b</sup> Ben-Gurion University of the Negev, Israel

<sup>c</sup> Hebrew University of Jerusalem, Israel

### ARTICLE INFO

#### Article history:

Received 27 March 2020

Accepted 17 April 2020

#### Keywords:

Shape modeling

Dihedral tessellation

Digital fabrication

### ABSTRACT

The growing popularity of 3D digital manufacturing has spurred a high demand for accessible methods for designing and fabricating customized 3D objects. In this paper, we present a novel approach to model and fabricate Escher dual-shape tilings from user-defined shapes. In a nutshell, Escher's dual shape tiling method smoothly transforms one tile pattern into another, generating a dual perception effect of the two shapes. We adapt Escher's dual shape tiling and perception effect to 3D manufacturing. Thus, our method takes two user-defined shapes and computes their dual shape tiling. A key feature of our method is that the dual shape patterns utilize solid and hollow spaces simultaneously. Specifically, our technique maps one shape to solid structure, while the second shape is mapped to hollow background, optimizing both spaces and bringing higher utilization of materials. To conform with 3D printability requirements, our tiling computation accounts for connectivity and strength as well as dense packing for efficiency. Our dual shape tiling algorithm gives rise to novel manufacturing applications such as ornamental texturing with dual perception Escher patterns, decorative window blinds, flexible tiling patterns, and shade effects.

© 2020 Elsevier Ltd. All rights reserved.

## 1. Introduction

3D manufacturing is rapidly progressing towards mass usage, with goals to enable non-professionals to easily manipulate and customize their 3D models into creative and beautiful products. Therefore, in recent years there has been significant research dedicated to providing computational tools for a wide range of shape manipulation and customization tasks for 3D printing. Among others, researchers have introduced novel techniques and applications such as balancing the manufactured shapes [1], creating spinnable objects [2], turning trees into printable models [3], stenciling decorative patterns [4], designing shapes as musical wind instruments [5], lampshades with projecting light control [6], models generating playful shadows [7], embedding QR codes [8] and helping users maintain printability during modifications [9].

In this paper, we study the modeling and fabrication of customized decorative patterns obtained by computing tilings of two shapes that coexist together. Dual shape tilings are mostly well-known from Escher's works, as a form of graphical art offering a dual perception mechanism. Specifically, the foreground-background assignment of neighboring shapes can reverse depending on the viewer's focal attention. Escher intentionally

employed dual figure-ground arrangements to reveal the ambiguities of visual perception and categorization. Their simplicity yet exciting perceptual effects, turned Escher's dual tiles into ubiquitous art and design structures [10].

In our work, we adapt Escher's dual tiles for artistic and decorative 3D printing purposes. Thus, we demonstrate their application to 3D manufacturing of decorative textured shapes. Our 3D tiles can be joined by hinges and connectors to form articulated Escher tilings. We utilize this dynamic pattern and apply it to create window blinds and dynamic structures that can be fabricated using a home printer. To the best of our knowledge, this is the first attempt to apply Escher's dual tiles to 3D manufacturing.

Decorative and artistic tools have been previously introduced in the context of 3D manufacturing. In general, these works, manipulate the printable 3D shape in search for novel applications to enrich 3D manufacturing. Nevertheless, the majority of these methods design artistic effects by focusing on the solid shape [11] or on the hollow space that emerges from the printed solid structure [6,7]. Our work, however, utilizes both solid and hollow spaces simultaneously. The method computes a dual shape tiling where the first shape is defined by the solid printed parts while the second shape emerges from the contour of the complementary background. The utilization of both solid and hollow spaces on the given surface introduces novel artistic and aesthetic effects as well as having the advantage of simplifying the overall structure and saving printing material.

\* Corresponding author.

E-mail addresses: [lxk811@gmail.com](mailto:lxk811@gmail.com) (X. Liu), [llu@sdu.edu.cn](mailto:llu@sdu.edu.cn) (L. Lu), [asharf@gmail.com](mailto:asharf@gmail.com) (A. Sharf), [io.yanxin@gmail.com](mailto:io.yanxin@gmail.com) (X. Yan), [danix@mail.huji.ac.il](mailto:danix@mail.huji.ac.il) (D. Lischinski), [chtu@sdu.edu.cn](mailto:chtu@sdu.edu.cn) (C. Tu).

The dual shape tiling is computed by optimizing the solid shape together with its complementary background while preserving visual shape properties such as contour and geometric features for each of the two shapes. To account for 3D printability, solid tiles, as well as complementary hollow tiles, should adhere to strength requirements. In our case, solid tiles should be partially connected using connectors wider than the minimum printing accuracy, while hollow parts should remain unconnected. We denote this condition as *mutual surroundings constraint*. We observe that this problem can be reduced to a dihedral tessellation problem in the plane under the constraint of mutual encirclement.

## 2. Related work

Our related work discussion is divided into surveying Escher tilings computation, manufacturing of tiling patterns and mosaics, and packing.

### 2.1. Escher tilings

A tiling of the plane is a collection of shapes that cover the plane without any gaps or overlaps. Dual tiling patterns a.k.a. “figure-ground” patterns may be observed as early as the nineteenth century in drawings of Koloman Moser. Most famous is M.C. Escher work in the first half of the twentieth century, which studied the regular division of the plane into tiles. In particular, he produced a large collection of ingenious tessellations [10], made from motifs resembling people, animals, and fantasy creatures. Following, Dress [12] has introduced a specific class of dihedral Escher tilings called “Heaven and Hell patterns” and Grünbaum and Shephard [13] have defined the mathematics behind tiling and geometric patterns.

“Escherization” was initially termed by Kaplan and Salesin [14] as a problem in computer graphics of tiling a plane with a given closed figure. The method modifies the given figure to conform to an isohedral tiling pattern. In a follow-up [15], authors extend their method to admit two shapes tilings using dihedral tiling patterns.

Yen and Séquin [16] developed a method to compute *Escher Spheres*, i.e., Escher tiles that are assembled on a sphere domain through a tiling deformation. Similar to us, Howison and Séquin [17] adapt Escher tiles for 3D manufacturing purposes. In their work, they investigate 2.5D isohedral tilings through extrusion and manual mesh editing. They also show 3D isohedral tilings using predefined lattices. In contrast, our technique is automatic and produces Escher dual-shape tilings that are 3D printable, allowing novel effects and applications.

Dual shape Escher tilings were explored [18] to generate a gradual transformation between the two shapes and obtain the dual perception effect. Escherization tiling has been formulated as a maximum eigenvalue problem to allow more intricate and complex tile shapes [19]. The shape optimization is also explored using interactive genetic algorithms [20] to find a shape for isohedral Escher tilings. In common to these works is finding a minimal modification for generating feasible single shape tiling patterns.

Recently Lin et al. [21] proposed a framework integrating matching and warping to generate Escher-like tiles transformations for dual shape perception. Our work has similar components addressing the dual shape tiling; however, ours is 3D fabrication oriented accounting for specific printability and application requirements.

### 2.2. Fabricable tilings

With the growing popularity of 3D digital manufacturing, researchers have paid much attention to the problem of

generating geometric patterns to decorate surfaces with the purpose of customization and enhancement of 3D printing.

Ornaments were applied to fabricated 3D objects by synthesizing 1D patterns along curves with restricted topology [22]. Similarly, synthesized printable 3D patterns were demonstrated by modifying texture synthesis to conform with a base surface [23]. Martinez et al. [24] synthesized flat shapes for laser cutting manufacturing and Chen et al. [25] synthesized filigree-like structures along surfaces. Their approach synthesizes a set of base elements along a target surface by preserving their appearance and allowing overlaps.

Zehnder et al. [26] introduced a method for interactive design with curve networks as ornamental priors onto 3D surfaces. In their work, the user positions curve elements onto a surface, which are then deformed using elastic rods simulation. Schumacher et al. [4] introduced a method to allow artistic cutouts into shell objects by removing material while accounting for printability and stability. Chen et al. [11] further proposed a method for synthesizing flat tile patterns on a base surface, such that the planar tiles can be easily printed and assembled afterwards. Recently Schüller et al. [27] introduced a novel fabricable-friendly tiling called “zippable”. In their work, they represent a 3D model with a single, long ribbon with a zipper around its boundary. In this approach, some distortion may occur to areas on the model. These works are concerned with mapping and printing 3D tilings onto arbitrary surfaces. Nevertheless, our technique involves 2D and 2.5D tilings in the plane, thus avoiding 3D mapping problems. Our method focuses on dual-shape tilings and the geometric relations between the solid and hollow parts in the manufactured patterns and their applications.

### 2.3. Mosaics tiles and packing

Mosaics are a form of art in which a large image is formed by placing together a collection of small images tiles. Photomosaics [28] are a collection of small images arranged in a rectangular grid in such a way that when they are viewed together from a distance, they suggest a larger image. Simulated Decorative Mosaic [29] approaches the problem of aligning square tiles with varying orientations to preserve input image edges while maximizing the area covered by the colored tiles.

Related to mosaics, tiling is the packing problem that has been extensively studied in computational geometry with application to a broad spectrum of layout problems, such as for cloth, leather, and glass. Since the packing problem is NP-hard [30], numerous heuristics have been developed. Kim and Pellacini [31] obtain a tighter mosaic packing by minimizing an energy function for a new kind of mosaics called Jigsaw Image Mosaic (JIM). To obtain the closest mosaic arrangement with no overlapping, Hu et al. [32] sample the surface according to the curvature and re-divide it using the chordal axis transform (CAT) obtaining optimal positions for the tiles elements. Kwan et al. [33] proposed a novel shape descriptor for computing the filling collage pattern. The major difference with our problem is that no adjacency constraints are considered in the above methods.

## 3. Overview

Given two user-defined shapes  $S_1, S_2$ , our algorithm computes an optimized dihedral tiling following four tiling rules while optimizing the shapes to account for tiling adjacency, printability requirements, and preserve their visual appearance.

Since the compatibility between  $S_1$  and  $S_2$  has a significant impact on the quality of the final result  $T_1, T_2$ , it is more convenient for non-professional users to manually specify  $S_1$  and let the system suggest a set of best candidates for  $S_2$  from a database.

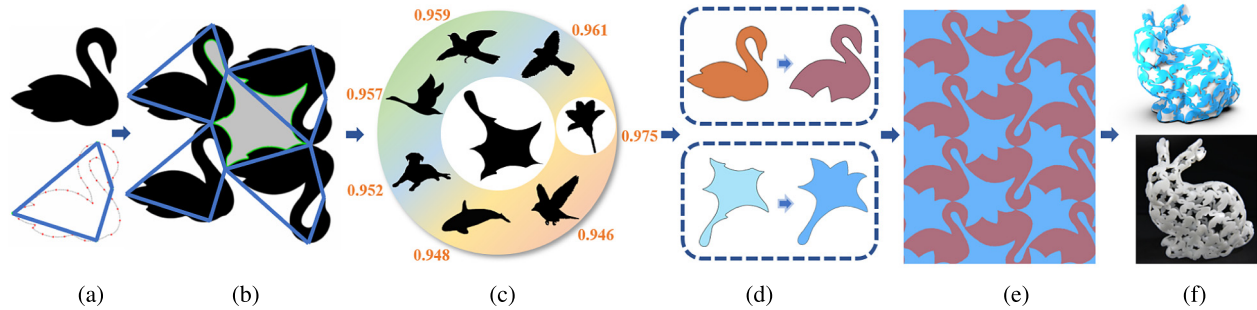


**Fig. 1.** Given a target shape and its quadrilateral polygon (a), we compute a rule-based four tiles pattern (b) and find the best matching shape to the enclosed tile from a database (c). We simultaneously morph the two shapes (d) such that they couple together, while preserving their visual appearance (d), resulting in a fabricable dual Escher tessellation (e) that can be mapped on a 3D object and efficiently manufactured (f).

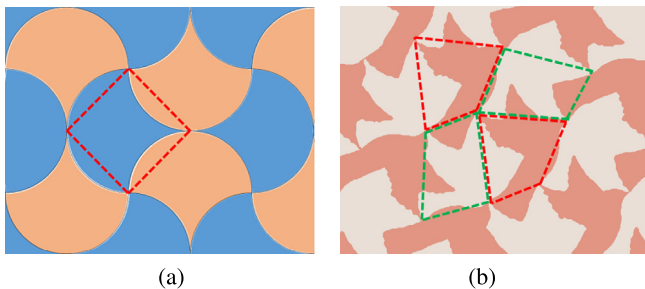


**Fig. 2.** Escher's artworks using Isohedral (a) and dihedral (b) tilings. Tiling polygons are marked by dash lines.

Both options are offered by our design framework and they share the same methodology.

Starting with one of the shapes  $S_1$ , we compute a quadrilateral polygon from its sample points. To compute a tiling of the plane from the initial quadrilateral, we define four tiling rules that satisfy the mutual surroundings constraints.

Next, we use the enclosed space  $M$  between the four tile shapes of  $S_1$  to define the complementary (hollow) dual shape pattern and match  $S_2$  to it. Then we morph this tiling configuration into the transformed shapes  $T_1, T_2$  such that they couple together and conform to printability requirements while preserving the visual appearance of the original shapes  $S_1, S_2$  as much as possible.

Our algorithm exhaustively searches for the best tiling pattern while simultaneously optimizing the two shapes to minimize their distortion and achieve an optimal tiling. The dual shape tiling can be applied as texture on a 3D surface to follow a 3D printing process. The algorithm pipeline is illustrated in Fig. 1.

## 4. Technical details

### 4.1. Dihedral tiling generation

A tiling of the plane is a collection of tiles that cover the plane without any gaps or overlaps. A tiling vertex is a point where three or more tiles meet. A tiling is dihedral if the tiling consists of two different tile shapes that are adjacent in the tiling (Fig. 2). We refer to [15] for further detailed definitions of dihedral tilings.

Our technique generates a two shape tiling where the first shape is contained in the foreground solid tile while the second shape is contained in the background similar to [21].

Starting with one of the shapes, we compute its corresponding quadrilateral tiling polygon by randomly selecting four points from the candidate points composed of feature points according to local curvature and uniformly sampling points between feature

points. Next, we define four tiling rules for placing the initial quadrilateral tiling polygon and generate a dihedral tiling pattern (see Fig. 3). Following these rules, the tiling pattern can be extended to the whole plane through repeated replications of the initial tile.

Essentially, these rules define a replication schemes of the initial tiling polygon into a grid-like four tile arrangement. The rules guarantee that the four tiles are touching each other, enclosing an isolated surface in their interior, which defines the dual background tile.

**Translation rule.** Translate  $P_1$  ( $P_i$  is the  $i$ th tile) along the diagonal vector  $\vec{13}$  ( $\vec{pq}$  is the vector from vertex  $\#p$  to  $\#q$ ) to obtain  $P_2$ . Translate  $P_1$  and  $P_2$  along the diagonal vector  $\vec{24}$  to obtain  $P_3$  and  $P_4$  respectively. (Fig. 3a).

**Flipping rule I.** Translate  $P_1$  along the diagonal vector  $\vec{24}$  to obtain  $P_3$ . Flip  $P_1$  and  $P_3$ , and translate along the diagonal vector  $\vec{13}$  to obtain  $P_2$  and  $P_4$  respectively. (Fig. 3b).

**Flipping rule II.** Translate  $P_1$  along the diagonal vector  $\vec{13}$  to obtain  $P_3$ . Flip  $P_1$  and  $P_3$ , and translate along the diagonal vector  $\vec{24}$  to obtain  $P_2$  and  $P_4$  respectively. (Fig. 3c).

**Rotation rule.** Rotate  $P_1$  around its tiling vertex  $\#1$  180 to obtain  $P_2$ . Rotate  $P_2$  around its tiling vertex  $\#2$  180 to obtain  $P_3$ . Rotate  $P_3$  around its tiling vertex  $\#3$  180 to obtain  $P_4$ . This rule is applicable only for parallelograms, otherwise the four elements cannot enclose a dual tile in their interior (Fig. 3d).

The above rules are a subset selection from the twelve “heaven and hell” tiling rules in [15]. Specifically, the translation rule corresponds to (IH01;1,4), flipping rules correspond to (IH03;2,5) and rotation rule corresponds to (IH47;2 $\frac{1}{2}$ ,4 $\frac{1}{2}$ ). Our motivation behind this selection of rules is that they generate nicely shaped quad tiles. Thus, they allow fitting shapes in their interior with minimal distortion.

Note that collisions between shapes may still occur when fitted to the quad tiles. In such cases, we avoid the specific tiling rule and keep only the valid tiling schemes.

### 4.2. Shape matching and morphing

With the above tiling rules, we search for the best matching tiling scheme followed by morphing the shapes to fit these tiles. Given a polygonal shape  $S_1$ , we uniformly sample its contour and compute its features at high curvature points. This yields a set of candidate tiling vertices.

We perform an exhaustive search, selecting each time four ordered points from the candidate set as a tiling polygon, generating quadrilateral tiling patterns according to our rules and computing a shape matching energy function. Our technique commences once a sufficient tiling has been found in terms of shape matching quality as measured by the energy function.

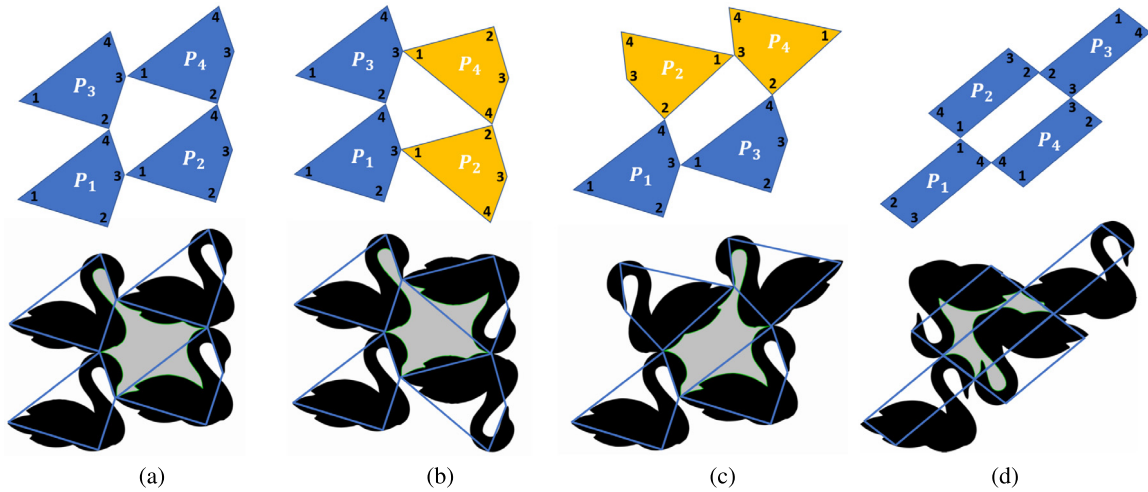


**Fig. 3.** Dihedral tiling rules: translation rule (a), flipping rule I (b), flipping rule II (c) and rotation rule (d). Upper row shows tiling polygons (flipped ones are in yellow) and lower row is the resulting tiling of the swan shape. (For interpretation of the references to color in this figure legend, the reader is referred to the web version of this article.)

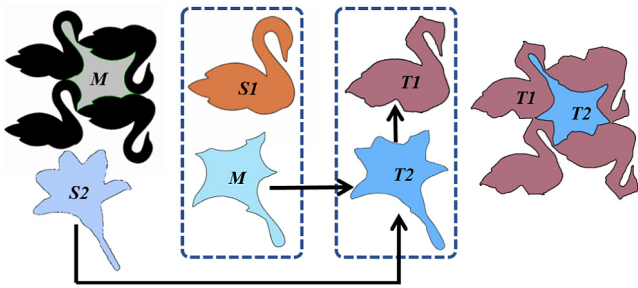


**Fig. 4.** Morphing. Starting from  $S_1$  and  $M$ , the optimized shapes  $T_1$  and  $T_2$  are obtained by morphing between  $M$  and  $S_2$ .

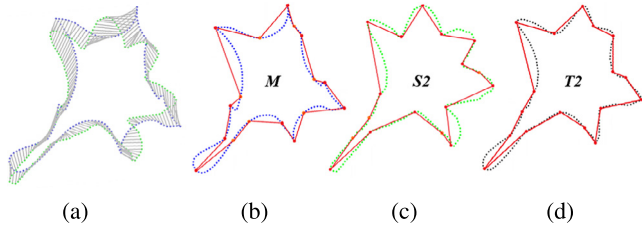


**Fig. 5.** Alignment of  $M$  and  $S_2$  based on shape correspondence (a); Frame polygons of  $M$  and  $S_2$  [34] (b, c, in red); Morphing result  $T_2$  (d). (For interpretation of the references to color in this figure legend, the reader is referred to the web version of this article.)

**Shape matching.** Matching  $S_1$  to a tile is straightforward as foreground quadrilaterals tiles are created by sampling four points in  $S_1$ . Therefore  $S_1$  and its tile simply match at those four points.

We denote the enclosed space between the four tiled shapes ( $S_1$ ) by  $M$ . The contour of  $M$  is extracted by connecting the tiling vertices in the pattern. For each tiling rule, we have a different order to preserve a consistent counterclockwise contour order (see Fig. 3).

Given the contour of  $M$ , we compute a best matching of  $S_2$  to  $M$ . If a database is given, our method retrieves a subset of top candidates according to their matching energy to  $M$ , and the user selects the most adequate shape as  $S_2$ .

To calculate the matching between two contours, we use the triangle-area representation (TAR) and measure with it the

similarity between matching points on the shapes contours [35]. This representation is effective in capturing both local and global characteristics of a shape, invariant to translation, rotation, and scaling, and robust against noise and moderate amounts of articulation. In the matching stage, we employ a dynamic space warping (DSW) algorithm to search efficiently for the optimal (least cost) correspondence between the points of two shapes.

To accelerate the whole shape retrieval process, we introduce a fast-reject filtering stage to avoid the costly similarity computation for too distinct shapes in the database. We use a 2D shape compactness – isoperimetric quotient signature, as our fast reject filter. It is defined as the ratio between the shape area and that of the circle having the same perimeter.

**Shape morphing.** Starting from the initial tiling configuration defined by the four tiles of  $S_1$  and the enclosed shape  $M$ , our aim is to find an optimal transformation of  $S_1$  and  $M$  into transformed shapes  $T_1$  and  $T_2$  with the objectives that they are as close as possible to  $S_1$  and  $S_2$  thus preserving their visual appearance (see Fig. 4).

We formulate the objective function to measure the visual quality of the transformed shapes  $T_1$  and  $T_2$  as follows:

$$E_{sim}(T_1, T_2) = \lambda F(T_1, S_1) + (1 - \lambda)F(T_2, S_2) \quad (1)$$

where  $\lambda$  allows weighing each shape deformation independently. In our experiments  $\lambda = 0.5$ , however if required could give higher priority to  $S_1$  over  $S_2$  thus increasing  $\lambda$ .  $F$  measures the degree of deformation from  $S$  to  $T$  and is defined as:

$$F(T, S) = \varphi(T, S) + Insec(T, S) - \omega'(T, S) \quad (2)$$

where  $\omega(T, S)$  is a shape similarity function based on TAR descriptors [35].  $\varphi(T, S)$  is the area function defined as:

$$\varphi(T, S) = (Area(T \cup S) - Area(T \cap S)) / Area(T \cup S), \quad (3)$$

$Insec(T, S)$  is a score that penalizes self-intersections in  $T$  or  $S$  with a high score in the range [1 – 2].

To minimize  $E_{sim}(\lambda, T_1, T_2)$  and maintain the coupling of  $T_1$  and  $T_2$ , we perform shape morphing between  $M$  and  $S_2$ . The shape  $T_1$  is defined from the distortion of  $T_2$  (specifically the tiling points) and the overall quadrilateral tiling pattern.

We employ the method of [34] to compute shape morphing, which is a two-level hierarchical interpolation algorithm. First,  $M$  and  $S_2$  should be aligned together based on the correspondence obtained from the shape matching stage (Fig. 5a). We compute

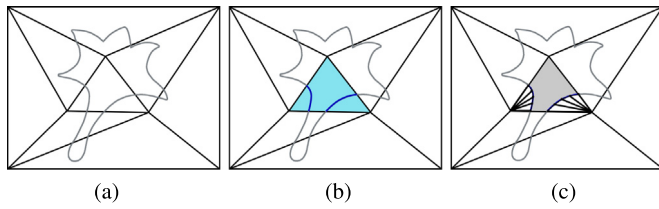


**Fig. 6.** Mesh difference. Input pattern contour overlaid on the mesh (a). Boolean difference between a triangle and the input contour (b) and the resulting constrained Delaunay triangulation remeshing the intersection region (c).

the frame polygons of  $M$  and  $S_2$  from the tiling vertices and feature points. Thus, we iteratively morph into intermediate shapes, to obtain the optimized result of  $T_1$  and  $T_2$  (Fig. 5b–c).

Note that the four tiling vertices stay fixed through the morphing process thus ensuring the connectivity of tiles in the final tiling. This is essential for printability requirements in the 3D manufacturing process.

### 4.3. 3D printable tilings

In the final step, we transfer our 2D dual tiling into a structurally sound 3D texture structure. For given a 3D model, we first compute its parametrization onto a 2D plane. Then, we compute a boolean difference between our tiling pattern and the two-dimensional triangular mesh. We generate the hollow parts corresponding the secondary shape in the tiling and reconstruct the surface. Finally we perform structural optimization to conform to printability requirements and obtain the target model.

**Mesh parametrization and boolean difference.** To map the input 3D mesh model onto a 2D parameter domain, we use the as-rigid-as-possible parametrization approach [36] since it preserves proportions of the tessellation structure and minimizes distortions.

We then overlay the 2D tiling pattern onto the parameterized mesh and compute the cutout difference between the surface mesh and the tiling pattern contour. We remove these cutouts and remesh the remaining surface mesh utilizing a constrained Delaunay triangulation (Fig. 6).

In the original tiling scheme, tilings connect to each other by tiling vertices that are not structurally stable for printability. We enhance stability by dilating contours, thus thickening the connectors between these contours. The conversion from points to connectors transform the hollow pattern into isolated components, which can be easily subtracted using the boolean difference to obtain a planar tiling of the triangular mesh.

Note that during the parametrization of closed shapes, they are cut into planar disk topologies yielding seams in the tiling pattern along these cuts. The parametrization of high genus models requires multiple cuts. Our parametrization technique aims at positioning these cuts in non-salient regions like the back or bottom of the model.

**3D printability and structural enhancement.** We map back the planar triangular mesh to three-dimensional space to obtain a 3D dual-tile shell model  $\mathcal{M}$  (i.e., a thick surface in 3D). Thus,  $\mathcal{M}$  is extruded by extruding each vertex along its normal direction (both positive and negative) by a default offset defining the shell thickness (in highly curved areas, self-intersections may occur when extruding the 3D shell model). The initial solid model  $\mathcal{M}_S$  is generated using Poisson surface reconstruction [37]. In all our experiments, the initial thickness is set to 1.2 mm to satisfy printing constraints.

To enhance the stability of the physical model, structural optimization is performed. First, we perform structural analysis via

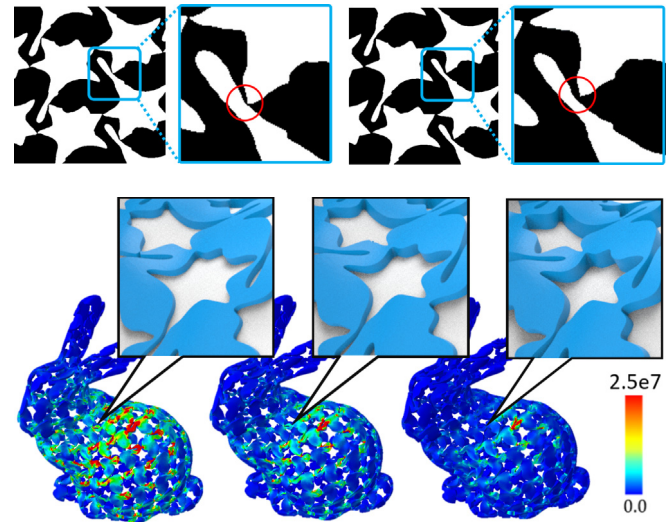


**Fig. 7.** Structural optimization. Top row, tiling vertices are enlarged in width for structural soundness. Bottom row shows iterations of local thickness optimization and the resulting stress distributions on the bunny model.

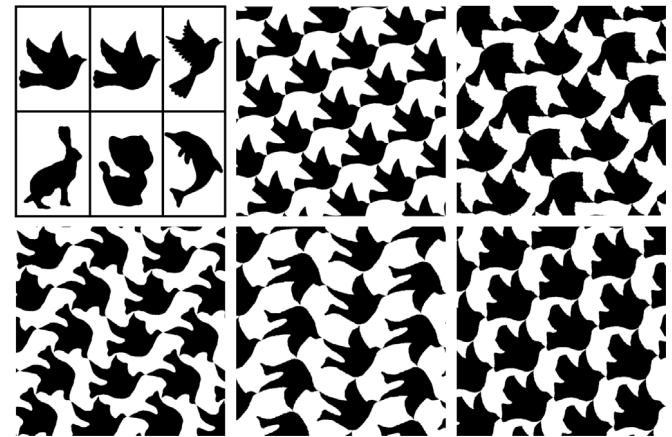


**Fig. 8.** Given a dove shape (top left) as input, our system generates the top five diedral tiling results. The matched shapes from the dataset are also listed at the top. The first result (top middle) takes the same shape as the dual.

finite element methods (FEM) on  $\mathcal{M}_S$  and obtain the von Mises stress for each element. To simulate stress, we fix the bottom part of the model and apply uniform pressure on the model. We use tetrahedral element here and employ the commercial software ABAQUS for stress analysis.

By default, we consider forces that are applied from all directions; however, specific strength requirements like pressing and holding may be easily incorporated in our optimization. E.g., in the bunny model in Fig. 7, we fix the bottom of the bunny and perform a 1000 N downward force on its back.

We perform a two-step optimization scheme to increase strength. First, we enforce connectivity between the weak part and its solid neighborhood through increasing the area of connectors. Next, we increase the thickness of the model for each weak surface vertex. We iteratively solve the optimization problem with the following objective function:

$$\operatorname{argmin} \mathcal{V}(\mathcal{M}_S(R(\mathbf{x}), D(\mathbf{v}))) \quad \text{s.t.} \quad SF(\mathcal{M}_S, \mathcal{F}) < \chi \quad (4)$$

where  $\mathcal{V}(\cdot)$  is the total volume of the foreground solid space,  $R(\mathbf{x})$  is the solid neighborhood of each tiling vertex  $\mathbf{x}$ ,  $D(\mathbf{v})$  indicates the thickness for each vertex  $\mathbf{v}$  on the mesh surface,  $SF(\mathcal{M}_S, \mathcal{F})$  is

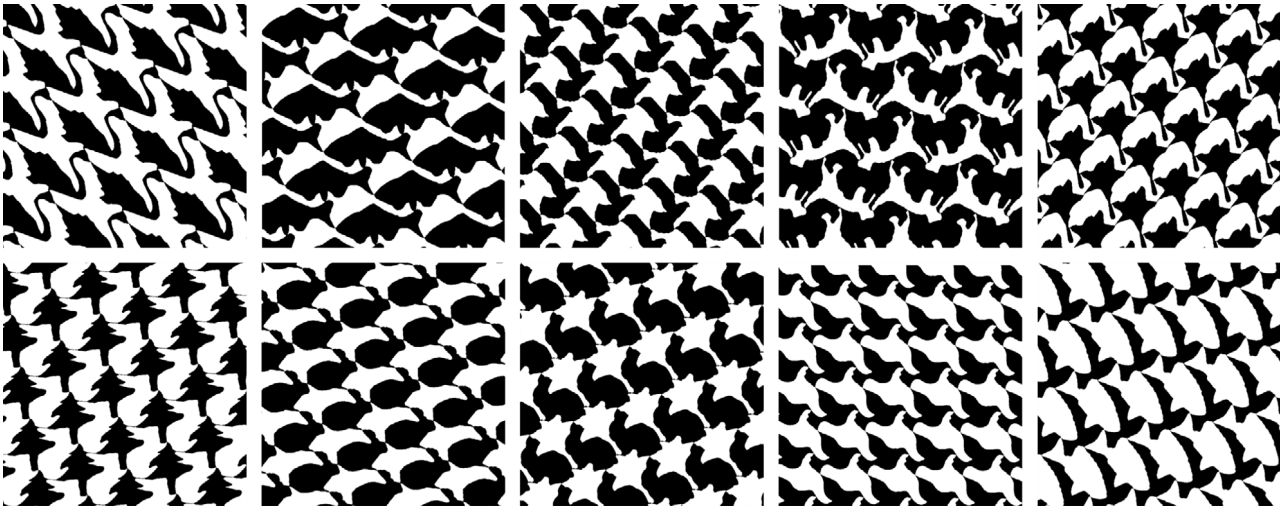


Fig. 9. Various dual-shape tiling patterns generated by our system.

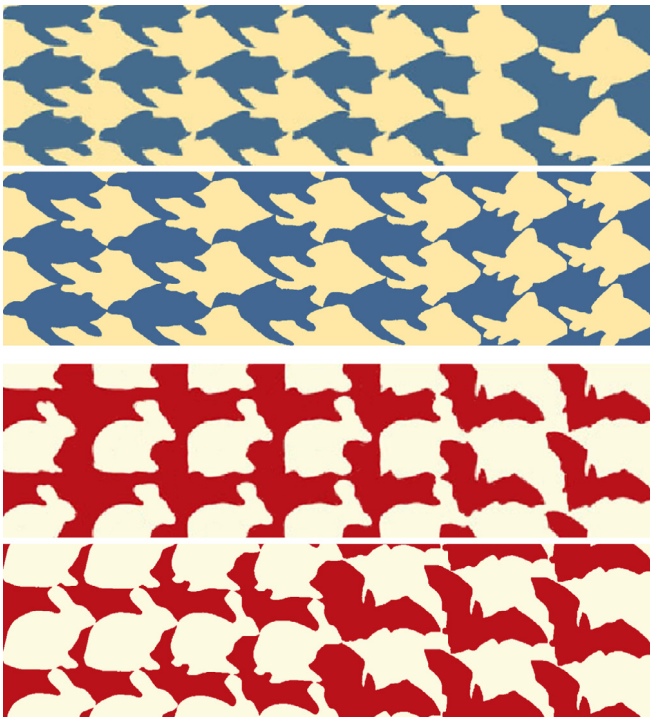


Fig. 10. Comparison between the results of [21] (upper row) and our results (lower row). In our results, the turtles and rabbits are connected, respectively.

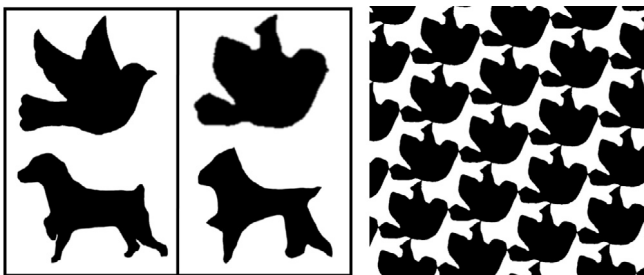


Fig. 11. A failure example. Left: two input shapes, dove (as in Fig. 8) and dog. Middle: the resulted deformed patterns. Right: the tessellation result.

the stress field computed from foreground solid model  $\mathcal{M}_S$  under the external forces  $\mathcal{F}$ , and  $\chi$  is the yielding value for the material ( $\chi = 20$  MPa for PLA in our experiments).

During the optimization, we first locally dilate the contour of the primary (solid) shapes in the weak areas to increase the connection area of the tiling vertices by a step size, until reaching the upper bound. The upper bound in connection area enlargement is 1% of the 3D shape's diagonal length. Then we increase the local thickness for the weak regions. We iteratively perform the two structural optimization steps, as shown in Fig. 7.

## 5. Results and discussions

We implemented our method and tested it on an Intel® Core™ i7-7700K CPU @ 3.6 GHz and 16 GB RAM. We have also created a database of shapes to allow the user to retrieve and select the best matching dual shapes for a user-defined primary shape. Our dataset is based on the MPEG-7 dataset [38], which we have enriched with additional images from the Internet. The dataset consists of 500 shapes, each represented by its polygonal contour.

*Performance.* Given one shape, our system suggests dual shapes for which the tiling best preserves visual appearance such that the users can select for further design (Fig. 8). This works better than asking the user to predefine two input shapes as it might need high artistic background.

Given a pair of shapes, it takes approximately 20 s to generate a tiling pattern. If a choice of best matching dual shapes is requested, shape retrieval for best matching candidates is a time-consuming query and scales linearly with the database size. In our experiments, querying our database of 500 shapes for a best matching dual shape for a given primary shape takes 30 min using the fast reject filtering. Fig. 9 lists some of the dihedral tiling patterns generated by our system.

Our method focuses on the shape geometry (i.e., the shape contour) as a means to preserve visual appearance. We compare our method dual tiling visual quality with [21]. We show in Fig. 10 a gradual deformation (transmutation) to achieve the sky-and-water pattern of [21]. The comparison shows that our method better preserves the contour geometry and thus the shape visual appearance and quality.

We note that given two arbitrary input shapes, the results may be less meaningful due to large deformations in the simultaneous optimization. Refer to Fig. 11. Thus, we recommend the users to assign one shape as the input and trust the dataset to obtain a set

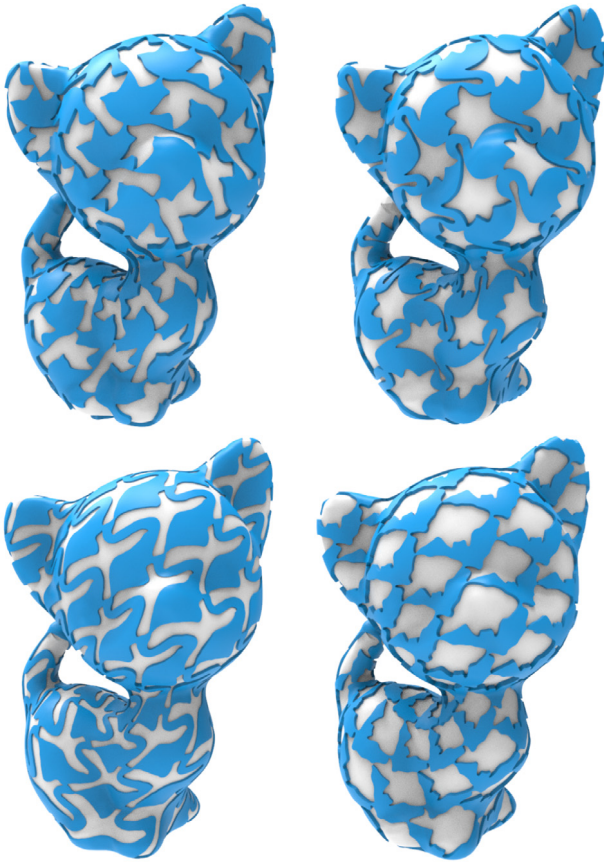


Fig. 12. Applying our printable Escher dual-shape tilings onto the 3D kitten.

of reasonable results. We also remark that the given shape cannot be a convex polygon.

**3D Fabrication and Applications.** We apply our dihedral tiling to the generation of customized 3D shape textures that can be 3D printed. Fig. 12 shows several 3D models with our dual shape textures.

Given the meaningful partitions of solid and hollow spaces, the dual patterns produce interesting light and shadow effects, which imply a great potential for designing customized lampshades. Fig. 13 shows 3D models textured with our dual shape Escher tiling. They are fabricated by an SLA-based printer and projected with custom lights to demonstrate the solid and hollow dual pattern effects. SLA or FDM based 3D printing for the decorative 3D models may require support structures. We did remove the

Table 1

Statistics of fabricated results (Fig. 13 from left to right). The size is represented as (length, width, height). Row #Tiles lists the number of hollowing tiles for each model.

Parameters	Kitten#1	Kitten#2	Bunny	Sphere
Size (cm)	(8,12.2,7.5)	(7,6.7,10.8)	(10.8,10)	(10,10,10)
Volume (cm <sup>3</sup> )	22.6	14.3	17.5	35
#Tiles	167	106	117	146

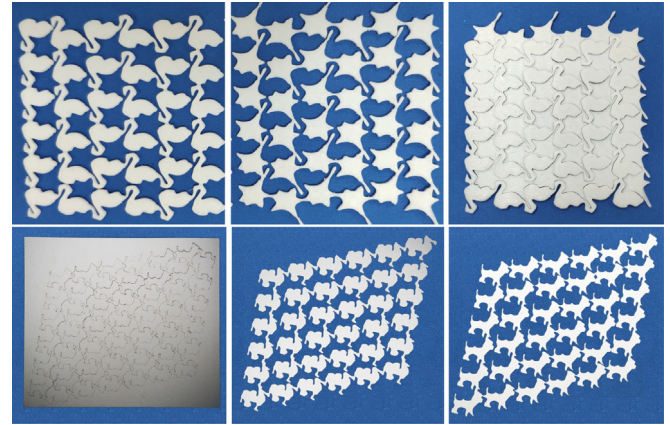


Fig. 14. Upper row: The swan and lily shapes are 3D printed in one piece, separately. Both pieces can combine together with full cover of the space. Lower row: The dual shapes are jointly fabricated by digital cutting and later separated into two connected pieces (camel and dog).

support materials for the four models manually, which is a bit tedious. Hence, we recommend dual-nozzle 3D printers with soluble support material, or powder-based 3D printing techniques such as SLS and Binder Jetting. Table 1 summarizes the statistics for the fabricated results.

We can also relax the mutual surrounding constraints for each tile, such that each element has connections with two neighbors that belong to the same shape type. Thus, both patterns can be fabricated in one connected piece, as shown in Fig. 14. This significantly speeds up the printing process of the dual tiles and allows for efficient utilization of the manufacturing process.

The interaction between the dual shapes and structures makes ground for novel applications. We demonstrate further applications along this path by adding joints to the connectors of some of the dual shapes. For example, given the swan-and-lily patterns, we add one rotation hinge (Fig. 15) to horizontal lily tiles. This allows the lily pattern to rotate with one degree of freedom simulating the behavior of window blinds. Blocking and control



Fig. 13. 3D printed models textured by our dual-shape tiling. A light source emanates through the hollow tiles in the pattern.

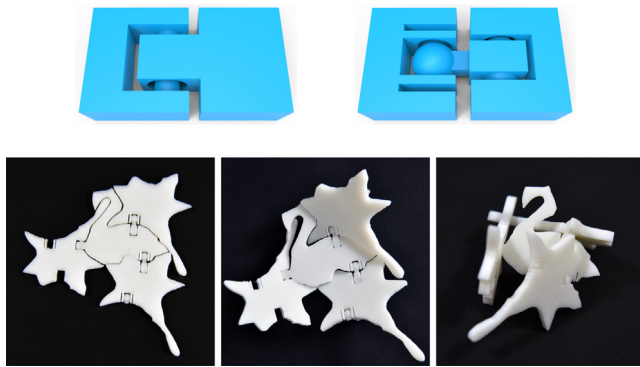


**Fig. 15.** Top: Two joints in our experiments. Left: Hinge joint; Right: Ball joint. Bottom: 3D printed dual shape tiles with ball joints allows a large degree of freedom and thus a variety of deformations.

of light using our 3D manufactured custom Escher blinds are demonstrated in Fig. 16.

We also add ball joints to our tiles (Fig. 15). A ball joint allows a limited range of smooth movement in all directions, and thus brings a larger degree of freedom for the patterns. Such joints are all support-free and can be 3D printed in one piece without postprocessing or meticulous assembly. Both models in Figs. 15 and 16 are fabricated by a standard desktop FDM-based printer.

Due to their controllability and continuous tessellation of the plane, dihedral tessellations are also natural candidates for halftoning. Since the tessellation structure is fixed, we control the halftoning amount by the tile scale parameter. Thus, we dilate tiles at different scales by controlling the distance between the center of the tile and the contour line of the target shape. The resulting halftone patterns are shown in Fig. 17.

## 6. Conclusions

In this paper, we present a novel approach to model and fabricate Escher dual-shape tilings from user-defined shapes. To conform with 3D printability requirements, our tiling computation accounts for strength and connectivity. A key feature of our method is that the dual shape patterns utilize both solid and hollow spaces. Thus, one shape is mapped to solid structure and the second shape is mapped to hollow background, optimizing both spaces simultaneously. The interaction between the dual shapes makes ground for novel applications. We demonstrate the applicability of our method to 3D textures with light shading, window blinds, deformable surfaces, etc.

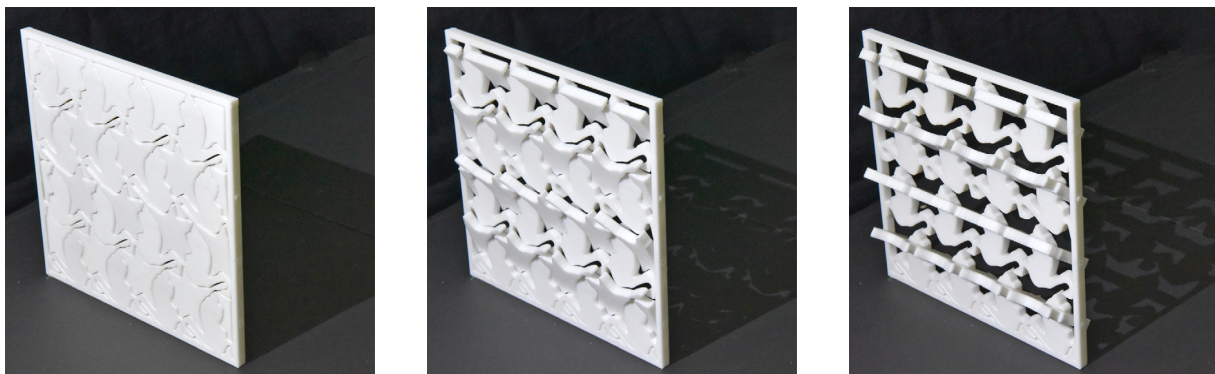


**Fig. 16.** The decorative window blinds made by adding hinges along horizontal tiles. Left to right, controlling the amount of light passing through by rotating the lilies blinds to allow more light.

**Limitations.** The current approach has several limitations. First, our technique utilizes a 2D parametrization of the 3D shapes in the computation of 3D printable dual tiles. In the case of complex topologies, parametrization may result in significant seams that affect the visual quality of our models. Although the seams are limited to less salient parts such as the bottom of the bunny, distortions due to the parametrization are sometimes inevitable, like the bunny's ears. Nevertheless, the problem of parametrization is orthogonal to our focus on fabricable dual Escher tiles. Second, the structural enhancement basically follows standard techniques. It would be more effective to integrate the structural optimization with the tile design framework. Thirdly, the types of tiling rules are relatively limited, yielding simplistic patterns. There are certainly more complex tiling rules that can be used to generate dense tessellations. Fourthly, the quality of the results strongly depends on the input shapes. If the user inputs some complex or special shapes, it may not be able to generate appropriate dense results. The last is that the interaction between different tiles due to joints positioning may yield collisions.

**Future work.** A natural future work direction is to incorporate parametrization and periodic dual tessellations in a unified optimization framework. Thus, we consider seams generations and the tiles periodic nature conjointly. This will allow positioning seams with minimal interference to the tiles periodicity. We would also integrate the strength enhancement with tiling design and consider optimizing the shape at a semantic level. Another possibility for future work is to explore more complex tiling configuration and to allow tiling with better appearance preservation. We are also excited by exploring novel applications for tiles with different joints. In general, generating exciting tiling deformations considering cloth deformations, wrinkles, and other different dynamic effects is a promising idea.

## Declaration of competing interest

The authors declare that they have no known competing financial interests or personal relationships that could have appeared to influence the work reported in this paper.

## Acknowledgments

We thank all the anonymous reviewers for their valuable suggestions. This work is supported by grants from NSFC, China (61972232, 61772318) and State Key Laboratory of Virtual Reality Technology and Systems, China (VRLAB2019A01).

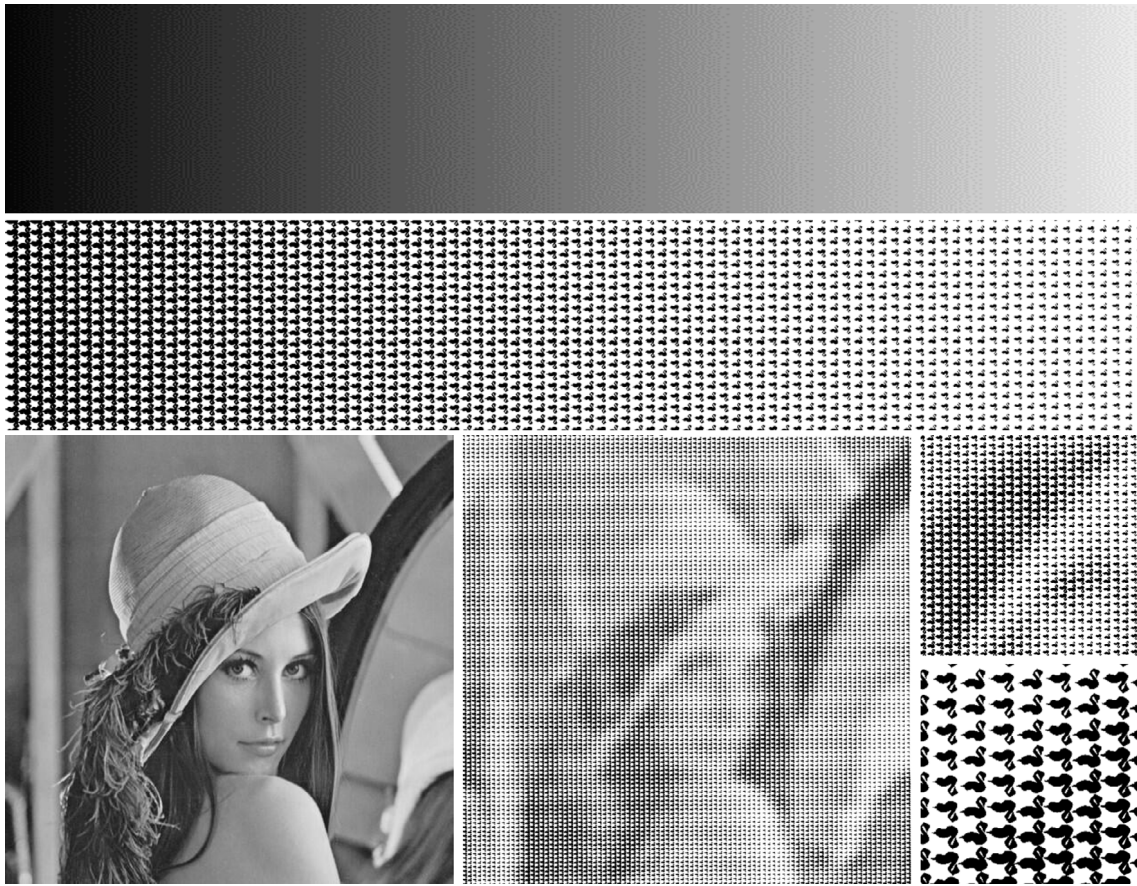


Fig. 17. Dual-shape tiles Halftoning.

## References

- [1] Prévost R, Whiting E, Lefebvre S, Sorkine-Hornung O. Make it stand: balancing shapes for 3D fabrication. *ACM Trans Graph* 2013;32(4):1. <http://dx.doi.org/10.1145/2461912.2461957>.
- [2] Bäcker M, Whiting E, Bickel B, Sorkine-Hornung O. Spin-it: optimizing moment of inertia for spinnable objects. *ACM Trans Graph* 2014;33(4):1–10. <http://dx.doi.org/10.1145/2601097.2601157>.
- [3] Bo Z, Lu L, Sharf A, Xia Y, Deussen O, Chen B. Printable 3D trees. *Comput Graph Forum* 2017;36(7):29–40. <http://dx.doi.org/10.1111/cgf.13269>.
- [4] Schumacher C, Thomaszewski B, Gross M. Stenciling: Designing structurally-sound surfaces with decorative patterns. *Comput Graph Forum* 2016;35(5):101–10. <http://dx.doi.org/10.1111/cgf.12967>.
- [5] Umetani N, Panotopoulou A, Schmidt R, Whiting E. Printone: Interactive resonance simulation for free-form print-wind instrument design. *ACM Trans Graph* 2016;35(6):184:1–184:14.
- [6] Zhao H, Lu L, Wei Y, Lischinski D, Sharf A, Cohen-Or D, et al. Printed perforated lampshades for continuous projective images. *ACM Trans Graph* 2016;35(5):154:1–154:11. <http://dx.doi.org/10.1145/2907049>, URL <http://doi.acm.org/10.1145/2907049>.
- [7] Mitra NJ, Pauly M. Shadow art. *ACM Trans Graph* 2009;28(5):156:1–7. <http://dx.doi.org/10.1145/1618452.1618502>, URL <http://doi.acm.org/10.1145/1618452.1618502>.
- [8] Peng H, Lu L, Liu L, Sharf A, Chen B. Fabricating QR codes on 3D objects using self-shadows. *Comput Aided Des* 2019;114:91–100. <http://dx.doi.org/10.1016/j.cad.2019.05.029>.
- [9] Shugrina M, Shamir M, Matusik W. Fab forms: customizable objects for fabrication with validity and geometry caching. *ACM Trans Graph* 2015;34(4):100:1–100:12. <http://dx.doi.org/10.1145/2766994>.
- [10] Schattschneider D. M.C. Escher: Visions of symmetry. W.H. Freeman; 1990.
- [11] Chen W, Ma Y, Lefebvre S, Xin S, Martínez J, Wang W. Fabricable tile decors. *ACM Trans Graph* 2017;36(6):175:1–175:15.
- [12] Dress AW. The 37 combinatorial types of regular “heaven and hell” patterns in the euclidean plane. In: MC Escher: Art and science. 1986, p. 35–43.
- [13] Grünbaum B, Shephard GC. Tilings and patterns. Freeman; 1987.
- [14] Kaplan CS, Salesin DH. Escherization. In: Proceedings of the 27th annual conference on computer graphics and interactive techniques. SIGGRAPH '00, New York, NY, USA: ACM Press/Addison-Wesley Publishing Co.; 2000, p. 499–510.
- [15] Kaplan CS, Salesin DH. Dihedral escherization. In: Proceedings of graphics interface 2004. GI '04, Canadian Human-Computer Communications Society; 2004, p. 255–62.
- [16] Yen J, Séquin C. Escher sphere construction kit. In: Proceedings of the 2001 symposium on interactive 3d graphics. I3D '01, New York, NY, USA: ACM; 2001, p. 95–8.
- [17] Howison M, Séquin CH. CAD tools for creating space-filling 3D escher tiles. *Comput-Aided Des Appl* 2009;6:737–48.
- [18] Sugihara K. Computer-aided generation of escher-like sky and water tiling patterns. *J Math Arts* 2009;3(4):195–207. <http://dx.doi.org/10.1080/17513470903185626>.
- [19] Koizumi H, Sugihara K. Maximum eigenvalue problem for escherization. *Graphs Combin* 2011;27(3):431–9.
- [20] Ono S, Kisanuki M, Machii H, Mizuno K. Creation support for escher-like tiling patterns by interactive genetic algorithms. In: SIGGRAPH Asia 2014 posters. SA '14, New York, NY, USA: ACM; 2014, p. 9:1.
- [21] Lin S, Morace CC, Lin C, Hsu L, Lee T. Generation of escher arts with dual perception. *IEEE Trans Vis Comput Graph* 2018;24(2):1103–13. <http://dx.doi.org/10.1109/TVCG.2017.2660488>.
- [22] Zhou S, Jiang C, Lefebvre S. Topology-constrained synthesis of vector patterns. *ACM Trans Graph* 2014;33(6):215:1–215:11. <http://dx.doi.org/10.1145/2661229.2661238>.
- [23] Dumas J, Lu A, Lefebvre S, Wu J, Dick C. By-example synthesis of structurally sound patterns. *ACM Trans Graph* 2015;34(4):137:1–137:12. <http://dx.doi.org/10.1145/2766994>.
- [24] Martínez J, Dumas J, Lefebvre S, Wei L-Y. Structure and appearance optimization for controllable shape design. *ACM Trans Graph* 2015;34(6):229:1–229:11. <http://dx.doi.org/10.1145/2816795.2818101>.
- [25] Chen W, Zhang X, Xin S, Xia Y, Lefebvre S, Wang W. Synthesis of filigrees for digital fabrication. *ACM Trans Graph* 2016;35(4):98:1–98:13.
- [26] Zehnder J, Coros S, Thomaszewski B. Designing structurally-sound ornamental curve networks. *ACM Trans Graph* 2016;35(4):99:1–99:10.

- [27] Schüller C, Poranne R, Sorkine-Hornung O. Shape representation by zippables. *ACM Trans Graph* 2018;37(4):78:1–78:13. <http://dx.doi.org/10.1145/3197517.3201347>.
- [28] Silvers R. *Photomosaics*. New York, NY, USA: Henry Holt and Co., Inc.; 1997.
- [29] Hausner A. Simulating decorative mosaics. In: *Proceedings of the 28th annual conference on computer graphics and interactive techniques - SIGGRAPH 2001*. ACM Press; 2001, <http://dx.doi.org/10.1145/383259.383327>.
- [30] Milenkovic V, Daniels K. Translational polygon containment and minimal enclosure using mathematical programming. *Int Trans Oper Res* 1999;6(5):525–54. <http://dx.doi.org/10.1111/j.1475-3995.1999.tb00171.x>.
- [31] Kim J, Pellacini F. Jigsaw image mosaics. *ACM Trans Graph* 2002;21(3). <http://dx.doi.org/10.1145/566654.566633>.
- [32] Hu W, Chen Z, Pan H, Yu Y, Grinspun E, Wang W. Surface mosaic synthesis with irregular tiles. *IEEE Trans Vis Comput Graph* 2016;22(3):1302–13. <http://dx.doi.org/10.1109/tvcg.2015.2498620>.
- [33] Kwan KC, Sinn LT, Han C, Wong T-T, Fu C-W. Pyramid of arclength descriptor for generating collage of shapes. *ACM Trans Graph* 2016;35(6):229:1–229:12. <http://dx.doi.org/10.1145/2980179.2980234>.
- [34] Yang W, Feng J. 2d shape morphing via automatic feature matching and hierarchical interpolation. *Comput Graph* 2009;33(3):414–23. <http://dx.doi.org/10.1016/j.cag.2009.03.007>.
- [35] Alajlan N, Kamel M, Freeman G. Geometry-based image retrieval in binary image databases. *IEEE Trans Pattern Anal Mach Intell* 2008;30(6):1003–13. <http://dx.doi.org/10.1109/tpami.2008.37>.
- [36] Liu L, Zhang L, Xu Y, Gotsman C, Gortler SJ. A local/global approach to mesh parameterization. *Comput Graph Forum* 2008;27(5):1495–504. <http://dx.doi.org/10.1111/j.1467-8659.2008.01290.x>.
- [37] Kazhdan M, Hoppe H. Screened poisson surface reconstruction. *ACM Trans Graph* 2013;32(3):1–13. <http://dx.doi.org/10.1145/2487228.2487237>.
- [38] Ralph R. MPEG-7 data set, <http://www.dabi.temple.edu/~shape/MPEG7/dataset.html>.